

Model Atmospheres for Low Field Neutron Stars

Mohan Rajagopal¹ and Roger W. Romani²

Physics Dept., Stanford University, Stanford CA 94305-4060

ABSTRACT

We compute model atmospheres and emergent spectra for low field ($B \lesssim 10^{10}$ G) neutron stars, using new opacity and equation of state data from the OPAL project. These computations, incorporating improved treatments of flux transport and convective stability, provide spectra for hydrogen, solar abundance and iron atmospheres. We compare our results to high field magnetic atmospheres, available only for hydrogen. An application to apparently thermal flux from the low field millisecond pulsar PSR J0437–4715 shows that H atmospheres fit substantially better than Fe models. We comment on extension to high fields and the implication of these results for neutron star luminosities and radii.

Subject headings:

1. Introduction

Thermal radiation from the surfaces of neutron stars (NS) provides important information about these elusive compact objects. In particular, neutron stars' thermal histories are already being probed by X-ray observations (Ögelmann 1995); these data place useful constraints on the interior physics and the equation of state of matter at super-nuclear densities (Tsuruta 1995). Significant limits on heating processes such as precipitation of magnetospheric particles and rotational energy dissipation in the crust can also be obtained. To interpret the observed X-ray fluxes, it is often assumed that the NS spectrum is blackbody. However in general we expect the emergent flux to be reprocessed by the NS atmosphere, and Romani (1987) showed that the departures from blackbody emissivities in the observed bands can be quite substantial.

In Romani (1987) opacities from the Los Alamos Opacity Library (LAOL) (Huebner et al. 1977) were used to generate model atmospheres and emergent spectra for non-magnetic neutron stars with a variety of surface compositions. More recent work (Shibanov et al. 1992; Potekhin & Pavlov, 1993) has treated the equation of state and opacity of pure H atmospheres in strong

¹mohan@astro.stanford.edu

²Alfred P. Sloan Fellow; rwr@astro.stanford.edu

($\sim 10^{12}$ G) magnetic fields. This allowed Pavlov et al. (1995) to produce atmosphere models for high field NS; substantial departures from blackbody spectra were found, albeit not as large as in the non-magnetic case. Since the atomic composition of a NS surface is quite uncertain it is also important to treat heavy element atmospheres. Miller & Neuhauser (1991) have calculated wave functions and energies of some magnetized heavy elements, and Miller (1992) produced polarization averaged bound-free cross sections and computed approximate model atmospheres. However, separate transport of the polarization modes dramatically affects the emergent spectrum (Pavlov et al. 1995), while at zero field bound-bound opacity can exceed bound free by large factors (Iglesias, Rogers & Wilson 1992), so these heavy element atmospheres may not adequately model the emergent spectrum. Thus since detailed treatments for elements heavier than H in strong fields are not yet available, comparison with low-field results remains useful.

To delimit the range over which our non-magnetic atmospheres can be applied, we must estimate the field required to perturb the opacity significantly at frequencies of interest. In the presence of strong magnetic fields, the free-free opacities for one of two polarization modes perpendicular to the field and for radiation parallel to the field are strongly suppressed. For Thompson scattering, the cross section decrease occurs below the electron cyclotron energy, i.e. $E_\gamma < h\nu_B = 11.6B_{12}$ keV, where $B = 10^{12}B_{12}$ G (Canuto, Lodenguai & Ruderman, 1971). For inverse Bremsstrahlung suppression, both E_γ and kT should be less than $h\nu_B$ (Pavlov & Panov, 1976); at typical NS temperatures of $\sim 10^6$ K, these effects would affect the ROSAT PSPC band (0.1-2.4keV) when $B_{12} > 0.01$. Magnetic effects on the bound-free and bound-bound opacities depend on the full quantum states of magnetized atoms, but some generalizations are possible. In the case of hydrogen, detailed calculations are available (e.g. Rösner et al. 1984); for the field $B_0 = 1.2 \times 10^9$ G, at which $h\nu_B = 1$ Ry, these authors find the ground state binding energy E_B is increased by $\sim 40\%$. Thus this bound-free feature too is altered when $h\nu_B \sim E_\gamma$. The effect vanishes rapidly at lower fields, while for large fields we find their results give $E_B \sim (2.5B/B_0)^{1/3}$ Ry. To estimate the minimum perturbing field in general, consider the magnetic contribution to the Hamiltonian of a hydrogenic atom (Rösner et al. 1984):

$$H_{\text{mag}}/1\text{Ry} \equiv H_1 + H_2 = 2\beta(m \pm 1) + \beta^2 r_\perp^2 \quad (1)$$

where $\beta = B/(4B_0)$, m is the quantum number for angular momentum in the field direction, ± 1 is for the spin, and r_\perp (in units of Bohr radii) is the atomic radius perpendicular to B . Here H_1 is the Zeeman effect, while H_2 is sometimes referred to as the quadratic Zeeman effect. For an energy level E_B with principal quantum number n_p and a nucleus with charge $+Z$, we define the critical field β_c to be that which gives $H_{\text{mag}} \sim E_B$. Using $r_\perp \sim n_p^2/Z^2$ and $E_B \sim Z^2/n_p^2$ Ry we find that $H_1 \sim E_B \implies \beta \sim (Z/n_p)^2$ (for $m \pm 1$ of order unity), and $H_2 \sim E_B \implies \beta \sim (Z/n_p)^3$. When $n_p > Z$, $H_2 > H_1$ and so the critical field scales as n_p^{-3} . This scaling is borne out by the results of Rösner et al. (1984) for excited states of Hydrogen. However, in NS atmosphere conditions only modest excitation of a species is obtained before it is further ionized, so for larger Z the perturbation H_1 dominates in almost all cases. Its dependence implies that spectral features will be perturbed when $h\nu_B \sim E_\gamma$, in agreement with Miller & Neuhauser (1991), who find for

hydrogenic atoms of atomic number Z that the lowest energy levels follow $E_Z(B) = Z^2 E_H(B/Z^2)$, where E_H is the corresponding hydrogen energy level at field B/Z^2 . They also find the helium ground state to follow this scaling, with a screened Z_{eff} . Line positions, which represent a difference between two energy states, will deviate substantially from their zero field values and ordering even before $h\nu_B$ reaches either energy, but a shell feature such as the iron L-edge at 0.7 keV in our spectra should persist to $B_{12} \sim 0.7/11.6 = 0.06$. Though the atmospheric structure will be affected for $h\nu_B > kT$ as the peak flux is altered, gross opacity features above the thermal peak will persevere to higher fields. Our non-magnetic atmospheres are therefore entirely suitable for low-field ($10^8 - 10^{10}$ G) NS such as millisecond pulsars, and indicative of some spectral features at higher fields.

Two developments suggest that a re-examination of the heavy element, non-magnetic NS atmospheres is timely. First, improved treatments of astrophysical opacity using the OPAL code (Iglesias et al. 1992; and references therein) and by the OP collaboration (Seaton et al. 1994) have shown that the LAOL results substantially underestimate the opacity, especially for iron-group elements in the $\sim 10^5$ K temperature range. Use of the new opacities already seems to resolve several puzzles in stellar astrophysics, including discrepancies between observations of Cepheid pulsations and models based on LAOL data (see Iglesias et al. 1992). The improvements to the opacity and equation of state (EOS) are particularly important to the NS spectrum problem, as the photosphere in these atmospheres forms precisely at the densities and temperatures where the changes to the LAOL results are largest. Secondly, recent observations have resulted in a number of strong (ROSAT) and potential (EUVE) detections of apparently thermal emission from nearby neutron stars, providing limited spectral information in the EUV/soft X-ray band. In particular, some low field (millisecond) pulsars have now been detected. It is clear that the next generation of space facilities in this band will provide significant constraints on NS thermal compositions and emissivities.

Thus to provide an improved baseline of models that illustrate spectral changes with surface composition and are directly applicable to low field neutron stars, we have constructed neutron star atmospheres and emergent spectra using the new opacities and consistent EOS, for pure iron, pure hydrogen, and the solar abundances of Grevesse & Noels (1993). Improvements in the radiative transfer are also introduced and the resulting spectra should supercede those of Romani (1987). Initial results of these computations have been reported in Romani, Rajagopal, Rogers & Iglesias (1995). In Section II we describe the calculation of the model atmosphere structures; in Section III we discuss convective stability of the atmospheres, and present emergent spectra. Spectra for various compositions are compared to black bodies and the high field hydrogen atmospheres of Pavlov et al. (1995). In Section IV we provide an initial application, fitting the spectra to ROSAT observations of the millisecond pulsar J0437–4715. Section V describes implications of these results and prospects for future work.

2. Model Atmospheres

2.1. OPAL Data

Because the EOS treatment allows extension to high density, OPAL EOS and opacity tables (kindly supplied by F. Rogers and C. Iglesias) are our primary data source for these models. OPAL opacity computations are based on the method of detailed configuration accounting using LS coupling (Iglesias, Rogers, & Wilson, 1987), and now use full intermediate coupling for iron to incorporate spin-orbit interactions (Iglesias et al. 1992). Abundances of all possible ions are obtained from an activity expansion of the grand canonical ensemble (Rogers 1986), and tables of the equation of state (EOS) completely consistent with that used for the opacity calculations are available (Rogers, Swenson, & Iglesias, 1995). For the present models, the EOS tables provide pressure and other thermodynamic variables as a function of temperature and density, interpolated using routines supplied with the data.

As an example, for pure iron the opacity grid was obtained for each decade of $R \equiv \rho/T_6^3$, where $T_6 = T/(10^6 \text{ K})$, from -5 to +1; with $\text{Log}(T)$ from 4.5 to 7.5 every 0.25, and with 10^4 photon energies linearly spaced over $0.002 < u \equiv E_\gamma/(k_B T) < 20.0$. As needed, we interpolate $\log \kappa$ linearly against $\log R$ and $\log T$ and linearly against u (at constant ρ and E_γ). To allow extension to high photon energies, we use additional tables for the same R and T spaced linearly in E_γ from 1eV to 10keV at 1eV intervals. These tables, used only when $E_\gamma > 20k_B T$, allow us to solve the transfer equation for E_γ up to 10 keV, through the lower temperatures present in the outer atmospheres. The data for the pure H and solar (Grevesse & Noels 1993) abundances are similar, densely covering the thermal peak with extension up to 1 keV.

2.2. Model Atmosphere Construction

We define *ab initio* a vector of 120 mean optical depths τ_T , logarithmically spaced between 10^{-3} and $10^{3.5}$. These correspond to physical depths through $dz = d\tau_T/\rho\kappa_T$, where κ_T is the total mean opacity in cm^2g^{-1} including electron conductivity (more below). The temperature and density at these grid points are adjusted until both hydrostatic equilibrium and energy steady state (total astrophysical flux $F = \sigma T_{\text{eff}}^4/\pi$) are achieved at all depths. For each of the three compositions, we generate six model atmospheres with T_{eff} from $10^{5.25}$ to $10^{6.5}$, four per decade. For the light element mixtures, the EOS tables stop before $\tau_T = 10^{3.5}$ in the two coolest atmospheres, and for iron in the one coolest and two hottest. In these cases, the depth grid extends to $\tau_T = 10^{2.5}$; this affects only the highest E_γ slightly.

At each frequency ν , the outward flux F_ν at the frequency-specific optical depth τ_ν is obtained from the Milne integral

$$F_\nu(\tau_\nu) = 2 \int_{\tau_\nu}^{\infty} S_\nu(\tau'_\nu) E_2(\tau'_\nu - \tau_\nu) d\tau'_\nu - 2 \int_0^{\tau_\nu} S_\nu(\tau'_\nu) E_2(\tau_\nu - \tau'_\nu) d\tau'_\nu \quad (2)$$

where S_ν is the radiation source function, and E_2 is the second exponential integral, which has maximum of one at zero, with decay length of order unity (Mihalas 1978). Similarly, the intensity J_ν is given by

$$J_\nu(\tau_\nu) = \frac{1}{2} \int_0^\infty S_\nu(\tau'_\nu) E_1 |\tau'_\nu - \tau_\nu| d\tau'_\nu \quad (3)$$

where E_1 is the first exponential integral. We assume Local Thermodynamic Equilibrium, taking the source of radiation at each depth to be a Planck function at the local temperature $B_\nu(T)$. The atmosphere models begin with the grey opacity solution $T^4(\tau) = (3/4)T_{\text{eff}}^4(\tau + q(\tau))$, using tabulated values for $q(\tau)$. In general, in a non-grey purely radiative atmosphere, at depths so large that radiative flux is given at all frequencies by the diffusion approximation

$$F_\nu = -\frac{4}{3} \left(\frac{1}{\kappa_\nu} \frac{\partial B_\nu}{\partial T} \right) \left(\frac{dT}{dz} \right), \quad \text{giving } F_{\text{rad}} = \int F_\nu d\nu = -\frac{16\sigma}{3\rho\kappa_R} T^3 \frac{dT}{dz}, \quad (4)$$

the grey solution is obtained on the optical depth scale defined by the Rosseland mean opacity. In the dense atmosphere of a neutron star, however, energy transport by electron conduction can be significant. We thus define an equivalent conduction opacity κ_c by analogy with equation (4) so that $-\lambda_c dT/dz = F_{\text{cond}} \equiv (16\sigma T^3)/(3\rho\kappa_c) dT/dz$, where λ_c is the thermal conductivity. Here we use $\kappa_c = (2.5 \times 10^4/N_e) (Z^2/A) (T_7^{1/2}/\rho) \text{ cm}^2/\text{g}$ where N_e is the number of free electrons per AMU, A is the average atomic mass, $Z = AN_e$ the average ionic charge, T_7 is in 10^7 K , and ρ is in g/cm^3 . Adding harmonically with the radiative opacity provides a total mean opacity $\kappa_T^{-1} = \kappa_R^{-1} + \kappa_c^{-1}$ on whose depth scale the initial grey model provides the correct atmosphere solution at large τ .

We start with the grey atmosphere temperature structure, and impose hydrostatic equilibrium starting at the surface ($P = 0$). For each τ_T layer, using an initial density ρ_0 from the layer above, we calculate the pressure at the base of that layer from $dP/d\tau_R = g/\kappa_R(\rho_0, T)$. We then obtain a corrected $\rho_1(T_0, P_0)$ from the EOS tables, and iterate to convergence. At each iteration, we extract the opacity on an 800 bin logarithmic frequency grid extending to 10keV, saving harmonic means of 50 OPAL opacities sampled within the bin. This grid of κ_ν values is used to produce the Rosseland mean opacity κ_R . Once convergence is reached at each depth, the final κ_ν and κ_R are saved, and similar arithmetic bin averages used to produce the Planck mean κ_P . Once hydrostatic equilibrium is achieved for the whole atmosphere, we solve the transfer equation (2) for each of the same 800 frequencies, first computing τ_ν corresponding to each of the 120 τ_T by integrating $d\tau_\nu = (\kappa_\nu/\kappa_R)d\tau_R$ down from the surface. At very large depth, where $S_\nu(\tau_\nu)$ varies slowly, we are in the diffusion limit and F_ν is obtained from equation (4); the intensity J_ν always comes directly from equation (3). Total flux F and intensity J are obtained by summing over the frequency grid, while the flux and absorption mean opacities κ_F and κ_J are obtained by appropriately weighted sums over the κ_ν .

The temperature structure is then corrected using the Lucy-Unsöld procedure to drive towards the desired steady state flux:

$$\Delta T(\tau) = \frac{1}{16\sigma T(\tau)^3} \left[\frac{\kappa_J}{\kappa_P} \left(3 \int_0^\tau \frac{\kappa_F(\tau')}{\kappa_R(\tau')} \Delta F(\tau') d\tau' + 2\Delta F(0) \right) - \frac{\kappa_R}{\kappa_P} \frac{d\Delta F(\tau)}{d\tau_R} \right], \quad (5)$$

(Mihalas, 1978) where $\tau \equiv \tau_T$ as defined above, and $\Delta F = \sigma T_{\text{eff}}^4/\pi - F_{\text{rad}} - F_{\text{cond}}$. The corrected temperature run is then smoothed and any temperature inversions in the outer atmosphere are removed. The procedure is iterated to convergence ($\pi\Delta F/\sigma T_{\text{eff}}^4 < 0.005$ at all depths).

3. Results

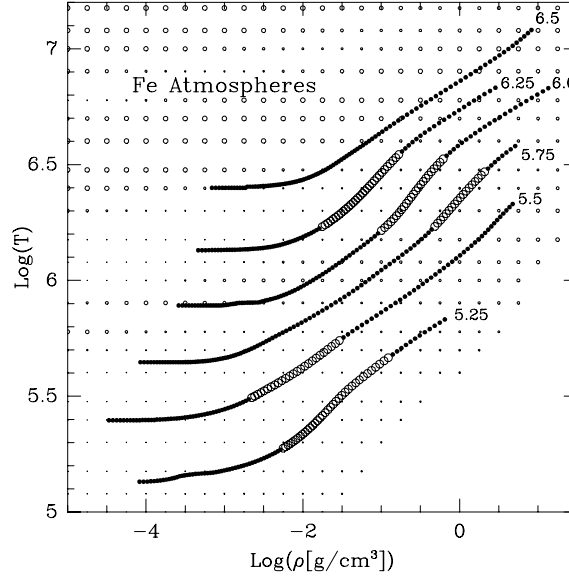


Fig. 1.— Iron atmosphere structures. Open circle regions of the curves are convectively unstable, and size of circles in the field indicates the adiabatic index of the gas.

We show the converged temperature vs. density runs for iron in Figure 1. Open circles indicate regions of convective instability, by definition where $(d \log T/d \log P)_{\text{atm}} \equiv \Delta_{\text{atm}} > \Delta_{\text{ad}} \equiv (d \log T/d \log P)_{\text{adiabatic}}$. The value of Δ_{ad} for iron from the EOS is indicated by the size of the background circles; instability in the radiative/conductive solutions occurs chiefly where it is low, in ionization zones. To gauge the importance of this instability we compute the energy gain ratio of a rising, but radiating, bubble

$$\Gamma \approx \frac{\kappa \rho^2 c_P}{24 \sigma T^3} l_{\text{mfp}} v \quad (6)$$

(*e.g.* Böhm-Vitense, 1992) where v is the mean bubble speed and we take the bubble mean free path l_{mfp} to be the atmospheric scale height $P dz/dP$. For small Γ , departures from the radiative temperature gradient scale as $9\Gamma^2/4$. If the bubbles rise freely and quasi-adiabatically, then equating the potential energy gain to the kinetic energy gives $v \sim [g(dT/dz|_{\text{rad}} - dT/dz|_{\text{ad}})/T]^{1/2} l_{\text{mfp}}$ as an upper limit to the bubble velocity. In this worst case picture, Γ is as large as ~ 5 at large depth in the $\text{Log} T = 5.75$ atmosphere. Accordingly the emergent flux at several keV, where τ_ν is modest at large depth, will be slightly affected. However, even the lowest known magnetic fields for neutron stars are $\sim 10^8 \text{G}$. If $B^2/8\pi > \rho g(dT/dz|_{\text{rad}} - dT/dz|_{\text{ad}}) l_{\text{mfp}}^2/T$, which is true

for $B > 10^7$ G throughout all the atmospheres we have computed, then the magnetic field will suppress the convection. Mass motions can then only occur on the diffusion time scale, which for a partly ionized plasma allows $v_{\text{diff}} \sim 1.1 \times 10^4 T_6^{-3/2} (1 \text{ cm}/l_{\text{mfp}}) \text{ cm s}^{-1}$. Under these conditions Γ is no larger than 0.04 except in the coldest iron atmosphere, in which convection might cause departure from the radiative temperature gradient at the 10% level. Accordingly, even when the magnetic field is too small to affect the EOS and opacities it should strongly suppress convection in most cases.

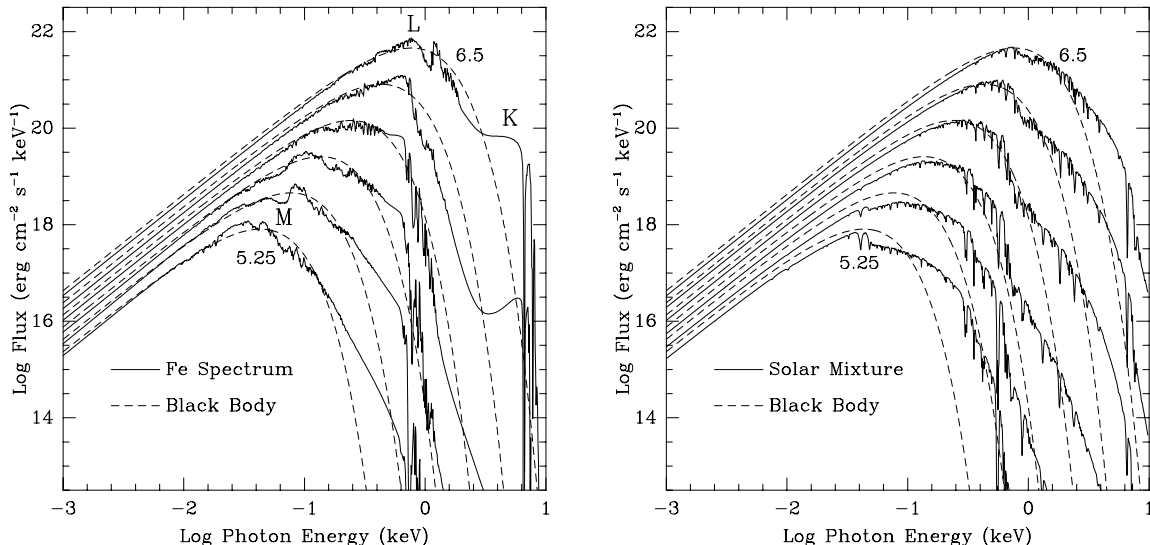


Fig. 2.— Emergent spectra for atmospheres containing heavy elements. See text for comments.

We calculate emergent spectra by solving the transfer equation at the edge of the atmosphere. To resolve lines from intermediate depths, we compute emergent spectra on a 2×10^4 point energy grid, logarithmically spaced between 1eV and 10keV. The spectra, binned down to 10^3 energies, are shown in Figure 2. Much coarser binning still is appropriate to the resolution of current NS observations, and as argued above, broad-band features will be stable even to moderate NS fields. The iron spectra all show features at the K, L and M edges, which are also present in the solar abundance spectra. Narrow absorption lines are formed at small physical depth, while strong pressure broadening affects lines from the deep layers. All three compositions are compared in Figure 3 (left); the hydrogen spectra show the expected hardening due to the ν^{-3} dependence of the opacity, which allows flux to shift above the Wien peak.

The two major spectral effects of magnetic field on hydrogen are visible in Figure 3 (right). First, the high energy hardening is not nearly as marked, since the diminished magnetic opacities which dominate transfer fall much less steeply than ν^{-3} (Shibanov et al. 1992, Fig. 1). Secondly, the higher photoionization threshold increases absorption between ~ 0.1 and 0.3 keV for the fields shown; the sharp onset is smoothed out by pressure effects on the atomic initial state (Pavlov et al. 1995). At the lower field, this effect causes the prominent dip in the $\log T = 5.5$ spectrum; at

$\log T = 6.0$ the dip is minimal, due to the lesser abundance of atomic hydrogen. At the higher field, only the onset is seen in the $\log T = 5.5$ spectrum, and it is clear this edge could dominate a fit.

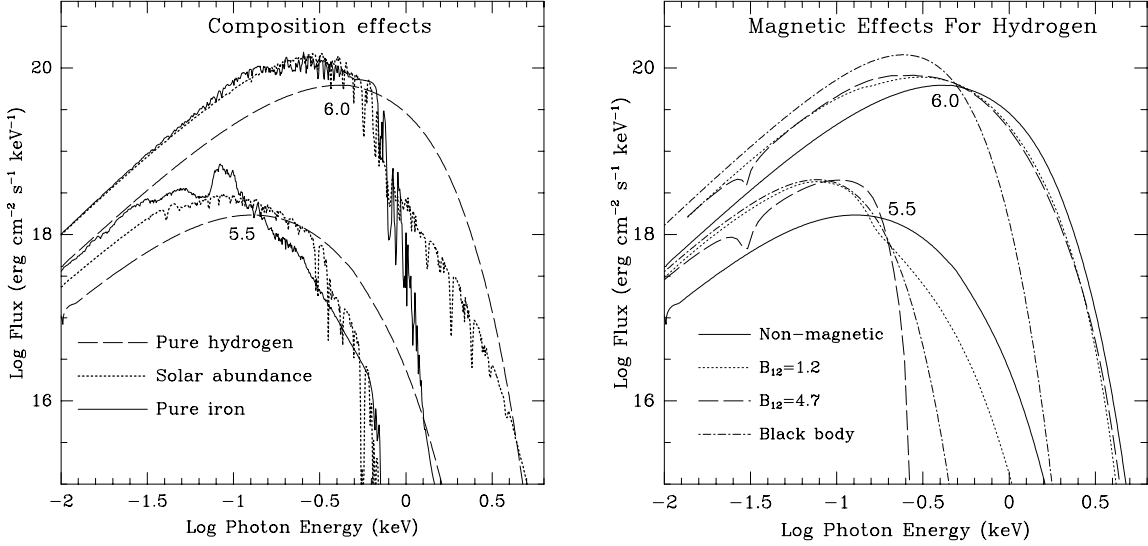


Fig. 3.— Left – comparison of different atmospheric compositions at two T_{eff} . Right – comparison of hydrogen spectra from the present work with the magnetic atmospheres of Pavlov et al. (1995).

4. Application

To apply these spectral results to soft X-ray data, we convert our spectra for each composition into a tabulated model for the XSPEC package. Our model supplies unredshifted flux at the NS surface. These spectra are subjected to a specified gravitational redshift, and overall normalization is fit as a free parameter. Model surface flux F_{NS} is related to model observed flux F_{obs} by:

$$F_{obs}(E_\gamma) = \frac{F_{NS}[(1+Z)E_\gamma]}{(1+Z)} \left(\frac{A_{em}}{\Omega D^2} \right) \left(\frac{1}{1+Z} \right), \quad (7)$$

where area A_{em} of the neutron star at distance D emits into solid angle Ω ; Z is the gravitational redshift, and the last factor due to time dilation. For full surface emission $\Omega = 4\pi$; if the star has a small emission region such as a heated polar cap we take $\Omega = 2\pi$, noting that limb-darkening would tend to decrease this value while gravitational light bending near the NS surface would cause it to increase.

As an example, we fit our models and magnetic hydrogen atmosphere emergent spectra for 1.2×10^{12} G and 4.7×10^{12} G, (Pavlov *et al.*, 1995), to a hypothesized thermal component in the X-ray emission of the nearby millisecond ($P = 5.7$ ms) pulsar J0437–4715 measured by ROSAT. Due to its low inferred surface dipole field of 8.3×10^8 G this is an ideal candidate, though its

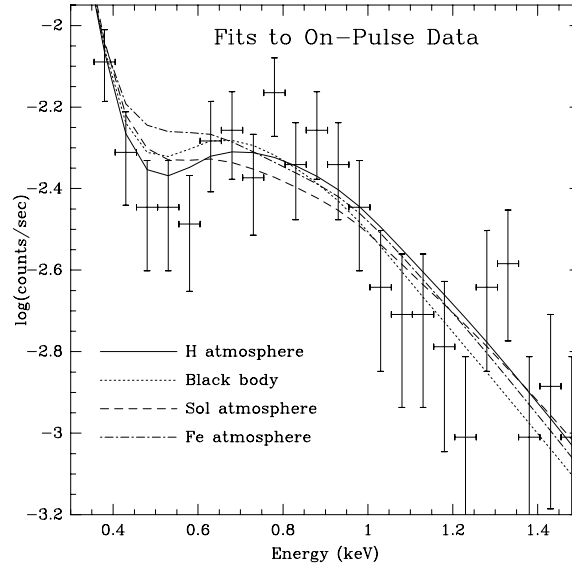


Fig. 4.— Best fits of model thermal components plus off pulse power law, to J0437–4715 ROSAT PSPC data in a crucial energy range. The model fits to the high-count soft peak below 0.3 keV are indistinguishable. Pi channels of the PSPC detector are here binned in groups of five, for display purposes only.

large spindown age $\sim 7.6 \times 10^8$ yr (Johnston et al. 1993) suggests that any thermal emission should come from reheating. We have re-analyzed the September 20-21 1992 PSPC data studied by Becker & Trümper (1993). This data set is in three segments, each of about 2000 seconds’ duration, the last two about one hour apart and separated from the first by about one day. We use 1300 photons from a circle 2 arcmin in radius centered at the X-ray position. Arrival times at the spacecraft clock are barycentred using standard IRAF PROS routines, and corrected for the pulsar’s orbital position using an updated radio ephemeris (Johnston et al. 1993; Bell, 1995). The nominal phase of the X-ray pulse in the last two segments aligns with the radio peak to within the ROSAT clock accuracy. An apparent ROSAT clock error after the first data segment required us to phase it separately, and make the necessary shift to align it with the other two. Based on the resulting light curve, we divide the data set into on- and off-pulse phases of equal duration; the on-pulse interval contains $\sim 60\%$ of the counts. While the clock error decreases confidence in absolute phasing somewhat, the measured alignment of the X-ray pulse with the radio peak (inferred from polarization data to be coincident with the neutron star magnetic axis; Manchester & Johnston 1995) supports the picture that this pulse represents thermal emission from a reheated polar cap. Hypothesizing that cap emission is superimposed on an unpulsed background magnetospheric or plerionic in origin, we fit a power law to the off-pulse data, finding a power law index of 2.5, with absorption column density of $1.1 \times 10^{20} \text{ cm}^{-2}$, in agreement with the results of Becker & Trümper (1993). We then added each thermal candidate model to the frozen power law with absorption held fixed, finding the best-fit parameters to the on-pulse data for blackbody

spectra, atmosphere spectra for our three compositions, and spectra from the magnetic hydrogen atmospheres. All models are processed through the current PSPC response matrix for comparison to the pi-channel data, and given $Z = 0.306$ redshift for a standard $1.4M_{\odot}$ neutron star 10km in radius. Fit parameters are determined via the maximum likelihood method using the C-statistic on unbinned data; the χ^2 for these fits are then determined from data binned to at least 20 counts per bin, with bin-width at least 1/3 the half-max width of the ROSAT energy response (Table 1). There are 12 DOF for the magnetic models, 11 for the others. Figure 4 shows the best fit models for black body and for each composition, smoothed through the detector response. Given the fitted normalization of the thermal component, we use equation (7), the radio dispersion pulsar distance of 140pc, $Z = 0.306$ as above, and $\Omega = 2\pi$ to infer the emission areas (Table 1).

Table 1: Fits to PSR J0437–4715 PSPC data

Model	$T_{\text{eff}}(10^6 \text{K})$	$A_{\text{eff}}(\text{km}^2)$	χ^2/DOF	$P(> \chi^2)$
BB	1.80	0.31	1.43	.205
H	0.60	22	0.95	.605
Fe	1.82	0.34	2.5	.002
Sol	1.4	0.73	1.5	.166
Mag(1.2)	1.0	4.3	0.91	.642
Mag(4.7)	1.0	4.2	0.93	.623

The fit for both atmospheres containing iron is significantly poorer because the strong L-edge (see Fig. 2) provides excess flux near 0.7 keV where the data show a deficit. Further, the model counts fall sharply above the edge where the data show an excess. The problem is exacerbated by redshifting the model edge to 0.6 or 0.5 keV. The BB and H fits are acceptable. Following our hypothesis that the thermal emission comes from re-heated polar caps, we can check the fitted effective areas against the cap area expected in the aligned dipole rotator model: the polar cap radius is $r_{\text{pc}} = r \sin^{-1}(r/r_{\text{lc}})^{1/2}$, where r is the pulsar radius and $r_{\text{lc}} = (Pc/2\pi)$ the light cylinder radius. In the case of J0437–4715, for $r = 10$ km we have $r_{\text{pc}} = 1.9$ km, giving $A \sim \pi r_{\text{pc}}^2 = 12 \text{ km}^2$. Only the H atmosphere fits give areas close to this standard polar cap; BB and Fe fits imply areas ~ 40 times too small. While the magnetic H fits and areas are acceptable, the $4 \times 10^4 \text{G}$ light cylinder field inferred from spindown torques would not allow surface $B \sim 10^{12} \text{G}$ unless the magnetic structure were of octupole order or higher. The resulting cap structure and thermal pulse would differ greatly from the dipole values inferred for PSR J0437–4715.

5. Conclusion

The behavior of NS spectra at energies high in the ROSAT band is crucial for temperature determination, as interstellar absorption often leaves only the Wien-like tail detectable. In that

case, the inferred temperature depends strongly on the composition model adopted: in most cases the atmospheric temperatures are substantially lower than those inferred for blackbodies, although high temperature Fe atmospheres may require a T_{eff} slightly higher than black body. Even with present limited spectral information and moderate absorption this composition dependence is significant. As an illustration, we have drawn sample ROSAT PSPC data sets as seen with absorption of 10^{20} cm^{-2} from our redshifted ($Z = 0.306$) models, and fit them with black body spectra. Figure 5 shows the ratios of fitted to actual temperature. For the $B_{12} = 4.7$ hydrogen atmosphere at it's lowest two temperatures, the black body temperature is driven down by the photoabsorption edge (above, and Figure 3). Standard cooling curves for neutron stars (e.g. modified URCA processes) run about four times hotter than curves for more exotic processes (e.g. direct URCA, pion condensates) before photon cooling takes over (Ögelman, 1995; Tsuruta, 1995) at $t \sim 10^6 \text{ y}$. Black body fits to thermal spectra from Ögelman's four initial cooling candidates place them quite near the standard curve, but Figure 5 demonstrates that even magnetic light element atmospheres could move their correct positions close enough to the cooler exotic process cooling to confuse matters considerably.

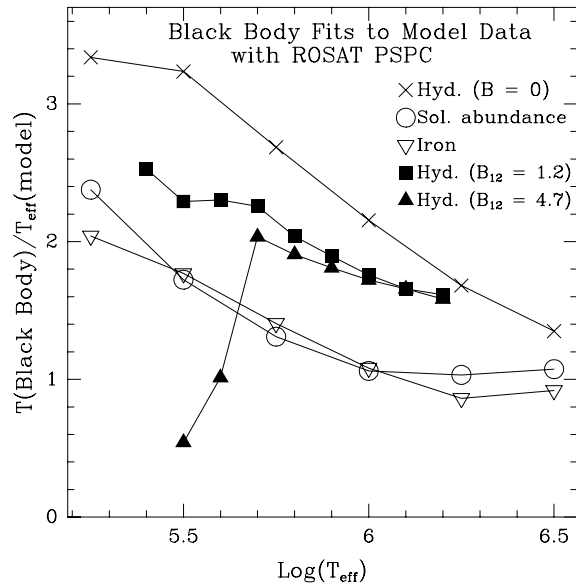


Fig. 5.— Fractional temperature error incurred when simulated 3000-count ROSAT PSPC observations of our model spectra are fitted with a black body.

Our emergent spectra are available in electronic form for the reader interested in determining flux implications for a particular band or detector, either as text files or as XSPEC models. For the pulsar J0437–4715, enough spectral information exists to break the composition/ T_{eff} degeneracy, favoring a pure hydrogen atmosphere quite strongly. The implied polar cap area is in much better agreement with theoretical expectation than that inferred from a blackbody fit. Future missions (e.g. AXAF & XMM) should be able to make similar measurements of other millisecond pulsars. Interestingly, non-magnetic fits to the ‘thermal’ emission of young, high-field pulsars seem in many

cases to favor H atmosphere models to blackbody spectra (Ögelman 1995 and references therein). While this agrees with the the compositional inference from PSR J0437–4715, comparison with heavy element magnetic atmospheres is needed to substantiate this result. A correct treatment of the detailed spectrum of such high B neutron star atmospheres will require extensive improvements to present atomic structure and opacity computations, although approximate models following broad-band features may now be feasible (work in progress). For younger pulsars, such models together with data from the next generation of X-ray satellites should enable a serious study of NS surface conditions, including composition, magnetic field and even redshift, with important implications for NS evolution and the EOS of matter at very high densities.

We are indebted to Forrest Rogers and Carlos Iglesias for computation of the OPAL data for the Fe models and assistance with their interpretation. We also thank G. G. Pavlov for providing high-field hydrogen spectra, I.-A. Yadigaroglu for assistance with the J0437 data, and the referee for a careful reading. RWR was supported in part by an Alfred P. Sloan fellowship and NASA grant NAGW-2963, and MR in part by a fellowship from the National Science and Engineering Research Council of Canada. This research has made use of data obtained through the High Energy Astrophysics Science Archive Research Center Online Service, provided by the NASA-Goddard Space Flight Center.

REFERENCES

- Becker, W. & Trümper, J. 1993, *Nature*, 365, 528
- Bell, J., 1995, private communication
- Böhm-Vitense, E. 1992, *Introduction to Stellar Astrophysics, Volume 3: Stellar Structure and Evolution*, (Cambridge Univ. Press:Cambridge)
- Canuto, V., Lodenguai, J., & Ruderman, M. 1971, *Phys Rev D*, 3, 2303
- Grevesse, N., & Noels, A. 1993, in *Origin and evolution of the Elements*, ed. N. Prantzo, E. Vangione-Flam, & M. Casse (Cambridge Univ. Press:Cambridge), 14
- Huebner, W. F., Mertz, A. L., Magee, N. H. Jr., & Argo, M. F. 1977, *Astrophysical Opacity Library*, Los Alamos Report LA-6760-M
- Iglesias, C. A., Rogers, F. J., & Wilson, B. G. 1987, *ApJ*, 322, L45
- Iglesias, C. A., Rogers, F. J., & Wilson, B. G. 1992, *ApJ*, 397, 717
- Johnston, S. et al. 1993, *Nature*, 361, 613
- Manchester, R. N. & Johnston, S. 1995, *ApJ*, 441, L65

- Mihalas, D. 1978, *Stellar Atmospheres*, (Freeman: San Francisco)
- Miller, M. C. & Neuhauser, D. 1991, *MNRAS*, 253, 107
- Miller, M. C. 1992, *MNRAS*, 255, 129
- Ögelman, H. 1995, in *The Lives of the Neutron Stars*, ed. M. A. Alpar, Ü. Kiziloğlu, & J. van Paradijs (Kluwer:Dordrecht) 101
- Pavlov, G. G. & Panov, A. N. 1976, *Sov Phys JETP*, 44, 300
- Pavlov, G. G., Shibbanov, Yu. A., Zavlin, V. E., & Meyer, R. D. 1995, in *The Lives of the Neutron Stars*, ed. M. A. Alpar, Ü. Kiziloğlu, & J. van Paradijs (Kluwer:Dordrecht) 71
- Potekhin, A. Yu. & Pavlov, G. G. 1993, *ApJ*, 407, 330
- Rogers, F. J. 1986, *ApJ*, 310, 723
- Rogers, F. J., Swenson, F. J., & Iglesias, C. A. 1995 preprint
- Romani, R. W. 1987, *ApJ*, 313, 718
- Romani, R. W., Rajagopal, M., Rogers, F. J., & Iglesias, C. A. 1996 in *IAU Colloquium 152, Astrophysics in the Extreme Ultraviolet*, ed. S. Bowyer & R. F. Malina (Dordrecht:Kluwer), 443
- Rösner, W., Wunner, G., Herold, H., & Ruder, H. 1984, *J. Phys. B: At. Mol. Phys.*, 17, 29
- Seaton, M. J., Yan, Y., Mihalas, D., & Pradhan, A. 1994, *MNRAS*, 266, 805
- Shibanov, Yu. A., Zavlin, V. E., Pavlov, G. G., & Ventura, J. 1992, *A&A*, 266, 313
- Tsuruta, S. 1995, in *The Lives of the Neutron Stars*, ed. M. A. Alpar, Ü. Kiziloğlu, & J. van Paradijs (Kluwer:Dordrecht) 133